Physiological Classification of Sympathetic Neurons in the Rat Superior Cervical Ganglion

Chen Li and John P. Horn

JN 95:187-195, 2006. First published Sep 21, 2005; doi:10.1152/jn.00779.2005

J Neurophysiol 95: 187–195, 2006.
First published September 21, 2005; doi:10.1152/jn.00779.2005.

Physiological Classification of Sympathetic Neurons in the Rat Superior Cervical Ganglion

Chen Li and John P. Horn
Department of Neurobiology, University of Pittsburgh School of Medicine, Pittsburgh, Pennsylvania

Submitted 22 July 2005; accepted in final form 15 September 2005

Li, Chen and John P. Horn. Physiological classification of sympathetic neurons in the rat superior cervical ganglion. *J Neurophysiol* 95: 187–195, 2006. First published September 21, 2005; doi:10.1152/jn.00779.2005. A new scheme is presented for identifying three sympathetic phenotypes in the rat superior cervical ganglion using electrophysiology and neuropeptide Y expression. Postganglionic compound action potentials recorded from the external and internal carotid nerves each contained two peaks, 1 and 2, with distinct preganglionic stimulus thresholds. Peak 2 in the external carotid response contained subpeaks 2a and 2b having a similar stimulus threshold. Neurons corresponding to peaks 1, 2a, and 2b were identified intracellularly by antidromic stimulation, graded preganglionic stimulation, injection with neurobiotin and immunostaining. Seventeen of 53 neurons studied this way had a low threshold for preganglionic stimulation of firing that corresponded to activation of extracellular peak 1. All low-threshold neurons were neuropeptide Y (NPY)-negative. The other 36 neurons had a high presynaptic stimulus threshold that corresponded to activation of extracellular peak 2, and 12 of these cells contained NPY. Together with other known features of ganglionic organization, the results indicate that low-threshold NPY-negative neurons are secretomotor cells projecting to salivary glands, that high-threshold NPY-negative neurons are pilomotor cells responsible for extracellular peak 2a, and that high-threshold, NPY-positive neurons are vasoconstrictor cells responsible for peak 2b. Secreto-, pilo-, and vasomotor neurons identified in this way had distinct axonal conduction velocities (0.52, 0.20, and 0.10 m/s) and diameters (33, 29, and 25 μm) but were indistinguishable in terms of preganglionic conduction velocities (0.30–0.34 m/s) and number of primary dendrites (8.4–8.6). The cell classification scheme presented here will allow future comparison of ganglionic integration in different sympathetic modalities.

INTRODUCTION

The superior cervical ganglion (SCG) is located at the rostral end of the paravertebral sympathetic chain and contains a mixture of neuronal phenotypes that selectively innervate different target organs located throughout the head (Gibbins 2004). These neuronal groups include cells that control specialized vascular beds in the brain, muscle, skin, and glands as well as piloerector hairs, salivary glands, the iris, and pineal gland (Arbab et al. 1986; Bowers et al. 1984; Flett and Bell 1991; Gibbins 1991; Gibbins et al. 1996; Morris et al. 1999; Reuss and Moore 1989; Uddman et al. 1989; Voyvodic 1989). In addition to target specificity, other physiological properties and anatomical features can serve to distinguish between different sympathetic phenotypes. These properties may play important functional roles and also be useful experimentally as markers for cellular identification. Thus for example, neuropeptide Y is selectively expressed by a large population of vasoconstrictor neurons in the SCG (Gibbins 1991; Jarvi et al. 1986) and by smaller populations of cells projecting to the iris (Bjorklund et al. 1985; Grkovic et al. 1999) and pineal gland (Reuss and Moore 1989). Studies of sympathetic ganglia other than the SCG indicate that functional subsets of neurons may have distinct axonal conduction velocities. This criterion forms the basis for identification of secretomotor B type neurons and vasoconstrictor C type neurons in bullfrog paravertebral ganglia (Dodd and Horn 1983a) and similarly has been shown to correlate with functional cell types in lumbar paravertebral ganglia of the cat (Janig and McLachlan 1992; Janig and Szulczyk 1981). The aim of the present study was to determine whether axonal electrophysiology and NPY expression could be used to identify functional subclasses of neurons in the rat SCG and then to compare synaptic convergence in different cell groups by counting the numbers of primary dendrites on neurons (Purves and Hume 1981; Purves and Lichtman 1985) that had been injected with neurobiotin.

We chose to study the problem of cellular identification in the rat SCG for a variety of reasons. By virtue of its location at one end of the paravertebral chain, one can isolate SCG preparations with distinct inputs and outputs. Preganglionic axons enter the ganglion through the cervical sympathetic trunk (CST), and the majority of postganglionic axons leave the ganglion through either the external carotid nerve (ECN) or the internal carotid nerve (ICN) (Bowers and Zigmond 1979). For this reason and because the head contains important targets, physiologists have long focused on synaptic mechanisms in the SCG (Eccles 1935; Feldberg and Gaddum 1934; Langley 1892; Skok 1973). The rat is an attractive animal model because its genetics are now well-defined (Gibbs et al. 2004), its nerves are large enough to manipulate, and the ganglion is small enough to image individual neurons under compound optics. Our approach combined extra- and intracellular recordings together with cellular fills, dendrite reconstructions, and immunocytochemistry. It thus became possible to identify individual cells in the caudal SCG as belonging to three discrete neuronal populations. We then examined phenotypic diversity in nicotinic convergence, a mechanism that could contribute to variations in the synaptic amplification of preganglionic activity (Karila and Horn 2000; Wheeler et al. 2004).

Address for reprint requests and other correspondence: J. P. Horn, Dept. of Neurobiology, University of Pittsburgh School of Medicine, E 1440 Biomedical Science Tower, Pittsburgh, PA 15261 (E-mail: jph@pitt.edu).

The costs of publication of this article were defrayed in part by the payment of page charges. The article must therefore be hereby marked "*advertisement*" in accordance with 18 U.S.C. Section 1734 solely to indicate this fact.

METHODS

Physiological methods

PREPARATION OF GANGLIA. Young adult male rats (Sprague-Dawley 180–250 g) were killed by CO_2 inhalation using procedures approved by the Institutional Animal Care and Use Committee at the University of Pittsburgh. Under a dissecting microscope, the SCG was removed together with a closely adhering 2-cm segment of the carotid artery. After pinning out the tissue in a 60-mm petri dish, the ganglion and associated nerves were carefully dissected away from the artery. The ganglion along with the CST and the ICN and ECN was then transferred to a recording chamber made from a 35-mm petri dish the bottom of which had been replaced with a round glass coverslip (31 mm, #1) and a thin 0.9-mm layer of silicone elastomer (Sylgard). The connective tissue capsule that surrounds the ganglion was then split open along its longitudinal axis and used to stretch and pin the preparation with a combination of cut down Minutien pins (100–150 μm diam, Austerlitz) and short lengths of 50-μm diameter stainless steel wire (hard temper AISI 302, Goodfellow Cambridge, Berwyn, PA). Careful stretching and pinning of the final preparation served to improve subsequent microscopy by flattening the ganglion and was essential for penetration of microelectrodes through the remaining connective tissue that surrounds all ganglionic neurons. Tight-fitting suction electrodes were then applied to the ganglionic nerves for extracellular stimulation and recording (Fig. 1), and the recording chamber was transferred to the stage of an upright fixed-stage Zeiss Axioskop microscope with ×40 Nomarski immersion optics.

PHYSIOLOGICAL SALINE AND SUPERFUSION. Throughout dissection and recording, the SCG was bathed in oxygenated mammalian Ringer solution that contained (in mM) 146 NaCl, 4.7 KCl, 2.5 $CaCl_2$, 0.6 $MgSO_4$, 1.6 $NaHCO_3$, 0.13 NaH_2PO_4, 20 HEPES acid, and 7.8 glucose (pH 7.3).

During recording, the preparation was superfused at 1–2 ml/min with a peristaltic pump (bath volume: ~1 ml). Most recordings were made at room temperature (23°C). For one series of extracellular recordings (Fig. 2), the bath was temporarily raised to 35°C using an SC-20 inline heater and CL-100 power supply (Warner Instruments, Hamden, CT).

EXTRACELLULAR AND INTRACELLULAR RECORDING. The suction electrode used to stimulate preganglionically through the CST was fabricated from Pt wire and polyethylene tubing. Electrodes made from chlorided Ag wire and plastic tubing were used to record extracellular postganglionic responses from the ECN and ICN (Fig. 1*A*) and also to stimulate antidromic action potentials (Fig. 1*B*).

For nerve stimulation, we employed brief (0.2 ms) electrically isolated pulses (A300/360, WPI, Sarasota, FL) with polarity adjusted for minimum response latency. Extracellular compound action potentials (CAPs) were recorded by connecting the ICN and ECN electrodes to two AC coupled differential amplifiers (Grass P15, West Warwick, RI). The extracellular amplifiers and the intracellular recording amplifier (Axoclamp 2B, Molecular Devices, Union City, CA) were connected to a common bath ground consisting of a Ag-AgCl pellet. Microelectrodes for intracellular recording were pulled from 1.2-mm fiber-capillary tubing, filled with 0.5 M KCl and 0.5% neurobiotin (Vector Labs, Burlingame, CA) and had resistances of 60–130 MΩ. All intracellular recordings were made under visual guidance from neurons on the surface of the ganglion. The data were monitored on an oscilloscope and digitized at 10 kHz using a Digidata 1200 computer interface and pClamp 7 (Molecular Devices).

Resting membrane potential (V_{rest}) was measured as the difference between the potentials immediately before and after withdrawal of the microelectrode from a cell. Only cells with $V_{rest} < -40$ mV and an overshooting action potential >60 mV in amplitude were included in the analysis. To calculate conduction velocities, conduction distances were divided by the latencies of ortho- and antidromic responses. The distances were measured by photographing each preparation at low power at the end of the recording session and measuring the shortest distances through the ganglion between extracellular suction electrodes (CST and ICN, CST and ECN) and between extracellular electrodes and sites of intracellular recording (Fig. 1).

NEURONAL FILLS. After successful electrophysiological study, neurons were injected with neurobiotin by passing 400–500 pA, 150-ms depolarizing current pulses at 1 Hz for 2–3 min.

Anatomical methods

MORPHOMETRY OF FILLED NEURONS. Generally, three to six neurons were filled in each experiment during 4–6 h of recording and their positions carefully noted. The SCG was then immersed for 1 h at room temperature in fixative containing 2% paraformaldehyde and 0.2% picric acid in 0.1M phosphate buffer (pH 7.3) and stored overnight in phosphate-buffered saline (PBS) at 4°C. The next day, the tissue was given three 10-min washes in 80% ethanol, followed by three 10-min washes in dimethyl sulfoxide and three 10-min washes in PBS. The wholemount was then incubated for 2 h at room temperature in streptavidin conjugated to CY3 (Jackson ImmunoResearch Laboratories, West Grove, PA) diluted 1:200 in PBS. After six 2-min washes in PBS, the ganglion was wholemounted in 1:1 glycerol:PBS on a glass slide and coverslipped.

To reconstruct neurobiotin-filled neurons, SCG wholemounts were photographed with an Olympus Fluoview FV1000 laser-scanning confocal microscope. The resulting Z-stacks of images were then transferred to a workstation and reconstructed using Imaris 4.0 software (Bitplane, Saint Paul, MN). The axon of each filled neuron was identified based on its length, which in some cells could be traced for

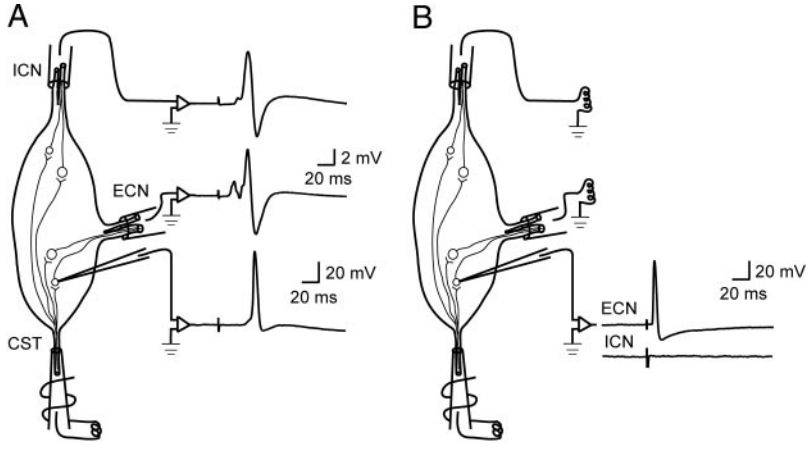

FIG. 1. Experimental arrangement for recording postsynaptic responses to orthodromic stimulation and antidromic stimulation. *A*: orthodromic responses to presynaptic stimulation of the cervical sympathetic trunk (CST) through a suction electrode. Suction electrodes on the external carotid nerve (ECN) and the internal carotid nerve (ICN) record postganglionic compound action potentials, and an intracellular microelectrode records excitatory postsynaptic potentials (EPSPs) that can initiate action potentials. *B*: the antidromic intracellular action potential evoked by postsynaptic stimulation of axons in the ECN and ICN. In this example, stimulation of the ECN but not the ICN elicits a response, thereby demonstrating that this neuron projects to the ECN. During experiments, suction electrodes on the ECN and ICN were switched as needed between the stimulating and recording configurations.

several hundred microns, and by the relative lack of branching. Rotating the three-dimensional reconstructions facilitated identification and counting of primary dendrites, using established criteria (Purves and Hume 1981). Dendrites were defined as nonaxonal processes that extended from the soma by >5 μm. In some neurons with complex shapes (Fig. 6), processes sometimes arborize very close to the soma. These were counted as a single dendrite when the branch point was <5 μm from the soma (Purves and Hume 1981). To measure the size of filled cell bodies, planar projections of reconstructed cells were imported into Zeiss Axiovision and traced. Somatic area (A) was converted to an equivalent diameter (d) by the relation $d = 2(A/\pi)$ exp0.5.

IMMUNOCYTOCHEMISTRY. After imaging filled neurons, ganglia were embedded, sectioned, and immunostained for neuropeptide Y (NPY). Each ganglion was rinsed three times in PBS, then dehydrated through graded ethanols and infiltrated with polyethylene glycol (PEG 1000) for 30 min under vacuum at 47°C. It was then embedded in molten PEG (MW 1450) and hardened at −20°C for 15 min. After embedding, the ganglion was cut into serial 10-μm sections on a Leica RM 2165 microtome. For immunocytochemistry, floating sections were rinsed in PBS, blocked for 2 h at room temperature in PBS containing 1.5% donkey serum (Jackson ImmunoResearch Laboratories) and 0.3% Triton-X100 (Sigma) and incubated overnight at 4°C in rabbit anti-NPY (Peninsula, San Carlos, CA), diluted 1:2,000 in blocking buffer. The sections were then rinsed in PBS and incubated in 1:200 donkey anti-rabbit CY2 (Jackson ImmunoResearch Laboratories) for 2 h at room temperature. After final rinsing in PBS, sections were mounted on glass slides, dried overnight, dehydrated through graded ethanols, cleared in xylenes, and coverslipped with Krystalon. Neurobiotin-filled neurons were then scored for NPY immunofluorescence under a Zeiss Axioskop 2 microscope and photographed (Axiocam HrC, Axiovision 4.2).

NPY immunoreactivity appeared as an intense ring of perinuclear staining, which in some but not all cells filled the cytoplasm. This pattern of staining replicates previous descriptions of NPY immunoreactivity in rat and mouse sympathetic ganglia [see Fig. 1 in Jarvi et al. (1986), Figs. 1*B* and 2*A* in Jobling and Gibbins (1999) and Fig. 1 in Headley et al. (2005)]. In addition to this characteristic subcellular distribution, there was a sparkly quality to NPY immunoreactivity that was easily distinguished from nonspecific background. All immunoreactivity was eliminated by omission of the primary antibody and by preabsorption of the primary antibody with 10 μM porcine NPY (Peninsula) for 18 h at 4°C.

Analysis and statistics

Grouped data are presented as the mean ± SD. Statistical differences between groups describing presynaptic conduction velocities, postsynaptic conduction velocities, cellular diameters, and numbers of primary dendrites were examined using a one-way ANOVA, followed by Tukey's test for multiple comparisons (Prism 4.0, GraphPad, San Diego, CA) and $P < 0.05$ as the criterion for significance. Figures were prepared using Igor 5.0 (Wavemetrics, Lake Oswego, OR), Adobe Photoshop CS, and Adobe Illustrator CS.

RESULTS

Postganglionic CAPs contain two major components

The extracellular CAPs that were recorded from the external and internal carotid nerves each contained two major peaks with distinct conduction velocities (Fig. 2, Table 1). Graded stimulation of the preganglionic CST demonstrated that the faster peak 1 had a lower stimulus threshold than the slower peak 2. Although the exact form of the two peaks varied from one ganglion to another, in 50 preparations, peak 1 was consistently smaller than peak 2 in both nerves. In addition, peak 1 was generally smaller in the ICN than in the ECN. Raising the temperature from 23°C (Fig. 2, *A* and *B*) to 35°C (Fig. 2, *C* and *D*) caused an approximate doubling of all conduction velocities (Table 1) but did not alter the basic appearance of peaks 1 and 2 or their relative stimulus thresholds. In many preparations, a notch divided peak 2 into subpeaks a and b (Fig. 2*A*), but these components had the same presynaptic stimulus threshold. The entire CAP was postsynaptic in origin because in separate control experiments it was reversibly blocked by 100 μM Cd^{2+}, an antagonist of voltage-dependent Ca^{2+} channels and by 10 μM dihydro-β-erythroidine, a nicotinic receptor antagonist.

These results suggest that the SCG contains at least two subpopulations of neurons the nicotinic synapses of which have distinct presynaptic stimulus thresholds. To test this possibility, we recorded intracellularly from neurons in the caudal ganglion that project to the ECN (Bowers and Zigmond 1979), which were identified by antidromic stimulation (Fig. 1*B*). We focused on ECN projecting neurons because peak 1 is larger in the ECN than ICN (Fig. 2). This suggests that neurons giving rise to the first peak would be most abundant in the caudal ganglion and therefore easier to find than low-threshold ICN projecting neurons, which are localized in the rostral ganglion.

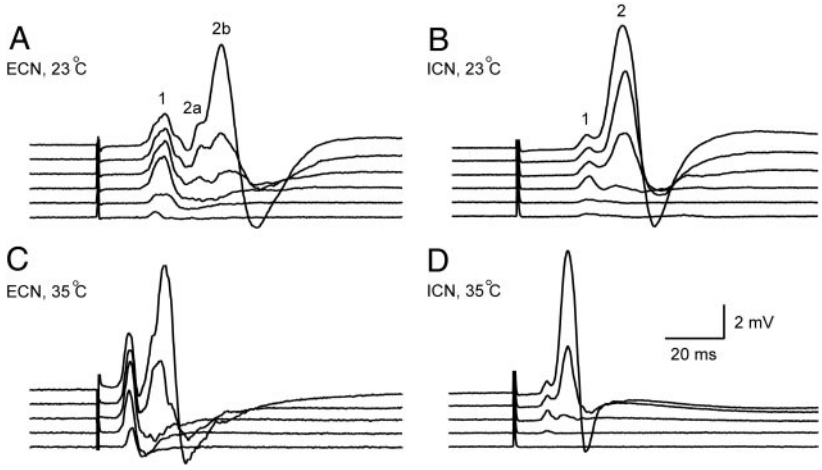

FIG. 2. Components of the postganglionic compound action potential (CAP) and their temperature dependence. Each panel illustrates a family of extracellular CAPs elicited by graded preganglionic stimulation of increasing intensity. *A* and *C*: responses recorded from the ECN at room temperature and 35°C. *B* and *D*: responses recorded from the ICN at these 2 temperatures. In all 4 panels, graded stimulation first recruits an early response defined as peak 1 and then a larger later response defined as peak 2. In the ECN recordings, peak 2 was often subdivided into subpeaks, labeled as 2a and 2b in *A*. These subpeaks had overlapping stimulus thresholds and were considered together as belonging to the high-threshold peak. Elevating the temperature to a physiological level, *C* and *D*, had the effect of speeding conduction but did not alter the basic appearance of peaks 1 and 2 or their relative stimulus thresholds.

TABLE 1. *Extracellular conduction velocities and their temperature dependence*

Postganglionic Nerve	CAP Peak	Conduction Velocity, m/s	
		23 °C	35 °C
ECN	1	0.40 ± 0.09	0.87 ± 0.11
	2a	0.28 ± 0.05	0.57 ± 0.09
	2b	0.21 ± 0.04	0.43 ± 0.06
ICN	1	0.34 ± 0.04	0.67 ± 0.10
	2	0.23 ± 0.03	0.42 ± 0.06

Conduction velocities were calculated using the latencies of peaks in the compound action potentials recorded from the external and internal carotid nerve (ECN and ICN) in response to supramaximal preganglionic stimulation of the cervical sympathetic trunk (n = 50). The scheme for numbering different peaks in extracellular records is illustrated in Fig. 2. Raising the temperature from 23 to 35°C caused a doubling in the conduction velocities of all action potential components.

Low- and high-threshold neurons

On average, sympathetic neurons in the rat SCG receive nicotinic synaptic input from 8.7 preganglionic neurons (Purves and Lichtman 1985). By carefully adjusting the strength of graded presynaptic nerve stimuli applied to the CST, we fractionated these converging preganglionic inputs into subthreshold and suprathreshold EPSPs (Fig. 3, *A* and *C*) and observed how this corresponded to recruitment of peaks in the extracellular compound action potential (Fig. 3, *B* and *D*). Consistent with previous studies (Hirst and McLachlan 1986; Jobling and Gibbins 1999; McLachlan et al. 1997, 1998; Skok and Ivanov 1983), we found that one or occasionally two of the nicotinic inputs were suprathreshold in strength. In some neurons, the presynaptic stimulus threshold for firing corresponded to peak 1 of the extracellular CAP (Fig. 3, *A* and *B*) and in other cells to peak 2 (Fig. 3, *C* and *D*). Using this correspondence, we classified neurons as being low- or high-threshold cells based on the minimal presynaptic stimulus required to trigger firing of a postsynaptic action potential. In cases where all of the inputs to a cell were examined, it was evident that some neurons received a combination of low- and high-threshold inputs. For example, Fig. 3*A* illustrates a low-threshold cell with a weak high-threshold input and *C* illustrates a high-threshold cell with a weak low-threshold input.

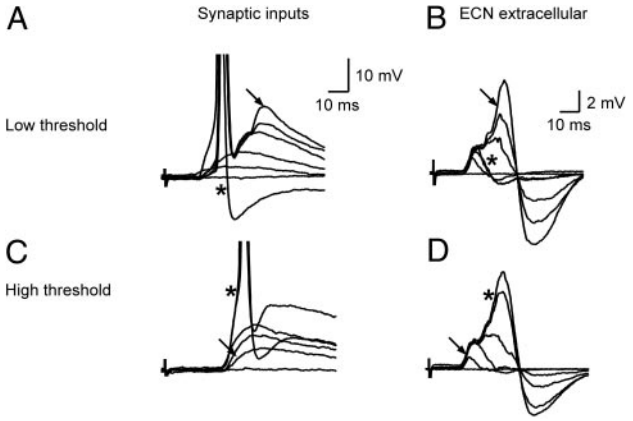

FIG. 3. Intracellular identification of low- and high-threshold neurons. Simultaneous intracellular and extracellular recordings at room temperature were used to determine how the stimulus thresholds for excitatory postsynaptic potential (EPSP) components corresponded to peaks in the CAPs recorded from the ECN. *A* and *C*: *, recruitment of a suprathreshold EPSP by graded presynaptic stimulation. *B* and *D*: corresponding extracellular responses. The low-threshold cell in *A* fired on activation of peak 1 in the extracellular recording in *B*. This contrasted with the high-threshold cell in *C*, which fired when peak 2 was recruited, *D*. These records also show that sympathetic neurons can receive combined low- and high-threshold synaptic input. ↓, *top row,* a high-threshold EPSP in the low-threshold neuron; *bottom row,* a low-threshold EPSP in the high-threshold cell.

NPY expression is restricted to a subset of high-threshold neurons

To determine whether the classification of neurons as low or high threshold correlated with other cellular properties that could help to establish functional identity, we broadened the study to include additional physiological and anatomical characteristics. We focused first on NPY, a postganglionic cotransmitter that is expressed primarily by vasoconstrictor neurons (Lundberg et al. 1982, 1984), a group that constitutes about half of all ganglion cells (Jarvi et al. 1986). When 53 ECN-projecting neurons were classified using presynaptic stimulus threshold and NPY immunoreactivity, only three of the four possible combinations were found (Fig. 4). None of the 17 low-threshold neurons contained NPY. This contrasted with the 36 high-threshold cells, which included a group of 12 NPY-positive neurons. With additional data from these neurons, we then compared the three cell types in terms of their axonal conduction velocities, numbers of primary dendrites and soma sizes (Figs. 5–7, Table 2).

Electrophysiological profiles of three neuronal types

The range of conduction velocities associated with peaks 1 and 2 in the extracellular CAP (Fig. 2) could arise from pre- or postsynaptic differences in axonal conduction velocities or from differences that were both pre- and postsynaptic.

To address this issue, axonal conduction velocities were calculated by measuring intracellular conduction latencies for

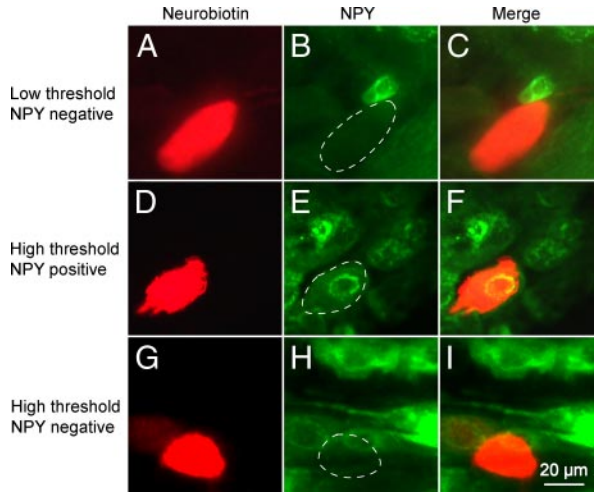

FIG. 4. Neuropeptide Y (NPY) is selectively expressed by a subpopulation of high-threshold neurons. ECN projecting neurons were identified by antidromic stimulation and classified by their presynaptic stimulus threshold for firing an action potential. They were then injected with neurobiotin and processed for NPY immunoreactivity. This approach led to the identification of 3 cell types, each illustrated as a row in this figure. *A, D,* and *G*: neurobiotin-filled cells. *B*, *E,* and *H*: NPY immunoreactivity with - - - highlighting the neurobiotin-filled cells. *C*, *F,* and *I*: merged images of the 2 labels.

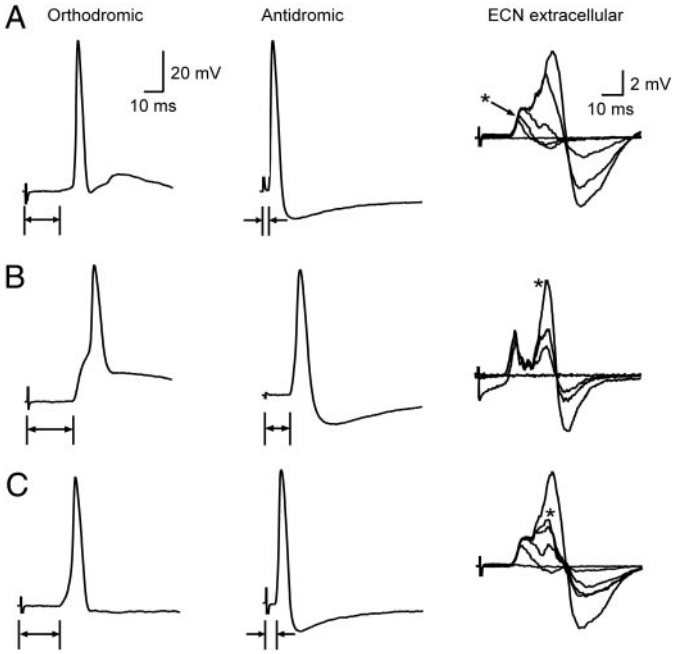

FIG. 5. Electrophysiological profiles of 3 neuronal types that project to the ECN. Each row in this figure illustrates the intracellular orthodromic and antidromic responses for a cell type together with extracellular recordings that were used to classify it as low- or high-threshold. *A*: a low-threshold, NPY-negative cell, *B*: a high-threshold, NPY-positive cell. *C*: a high-threshold, NPY-negative cell. ↔ drawn below the intracellular recordings, conduction delays. * in the CAP, the response used to classify the cell as being low- or high-threshold.

each of the three cell types (Fig. 5) along with conduction distances between stimulating and recording electrodes. This revealed that the slower conduction velocity of peak 2 in the CAP was mainly postganglionic in origin.

Due to the inverse relation that normally exists between extracellular stimulus thresholds and axonal conduction velocities (Keynes and Aidley 1991), one would expect low threshold neurons to have faster preganglionic conduction rates than high-threshold neurons. Although this trend was evident in our data (Figs. 3, *A* and *C,* 5, and 7*A,* Table 2), the differences were small and not statistically significant. This contrasted with postganglionic conduction velocities, which differed significantly between all three groups (Figs. 5 and 7*B,* Table 2). Postganglionic axons of low-threshold neurons had the fastest rates while high-threshold, NPY-positive cells had the slowest conducting axons. Resting potentials of the three cell types were indistinguishable (-50.1 ± 5.8 mV for low-threshold neurons, -50.9 ± 5.4 mV for high-threshold, NPY-positive neurons, -51.7 ± 7.4 mV for high-threshold, NPY-negative neurons).

By combining the intracellular pre- and postsynaptic conduction latencies and conduction distances, it was possible to calculate overall conduction velocities for the three cell groups (Table 2) and then compare them with the extracellular conduction data from ECN recordings (Table 1). This comparison confirmed that low-threshold neurons produce peak 1 in the CAP. It also revealed that high-threshold, NPY-negative neurons correspond to peak 2a and that high-threshold, NPY-positive neurons correspond to peak 2b.

Use of dendrite branching as an index of synaptic convergence

It was of interest to compare nicotinic convergence in the three cell types because convergence is an important determinant of synaptic amplification in autonomic neurons and could, in principle, differ between subclasses of neurons that serve different physiological roles (Karila and Horn 2000; Wheeler et al. 2004). To test this idea, neurons that had been electrophysiologically classified were filled with neurobiotin, and the number of primary dendrites on each cell was counted from

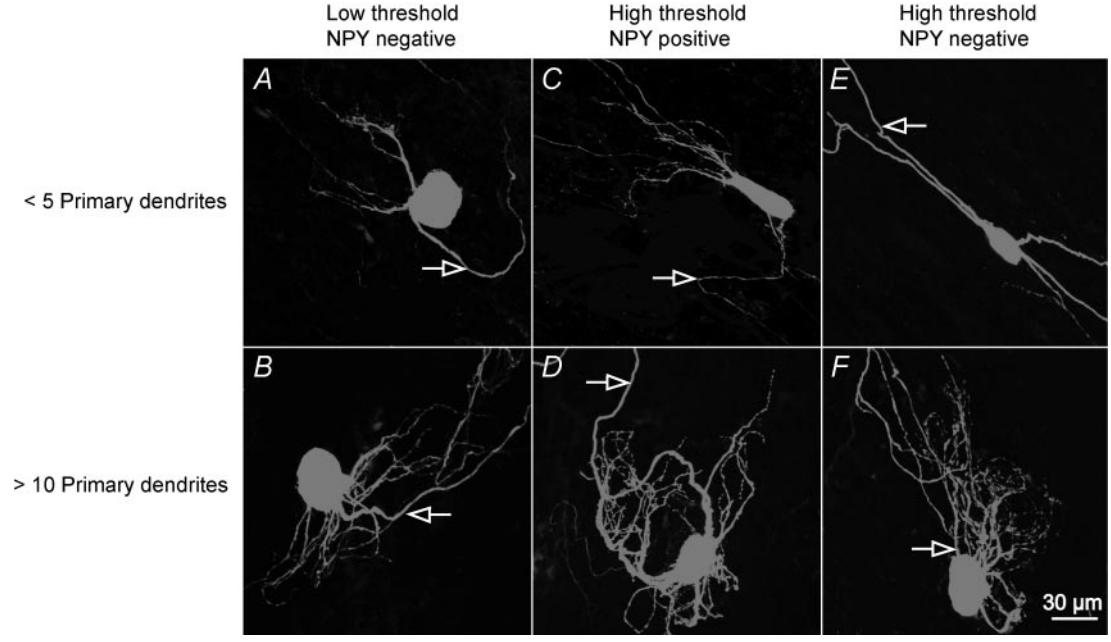

FIG. 6. Variations in dendritic complexity do not distinguish the 3 neuronal types. Confocal reconstructions of neurobiotin-filled ECN projecting neurons that were classified as low-threshold, NPY-negative (*A* and *B*), high-threshold, NPY-positive (*C* and *D*), or high-threshold, NPY-negative cells (*E* and *F*). For each cell type, there were some neurons with <5 primary dendrites, *A, C,* and *E* and others with >10 primary dendrites, *B*, *D*, and *F*. →, the axon of each neuron.

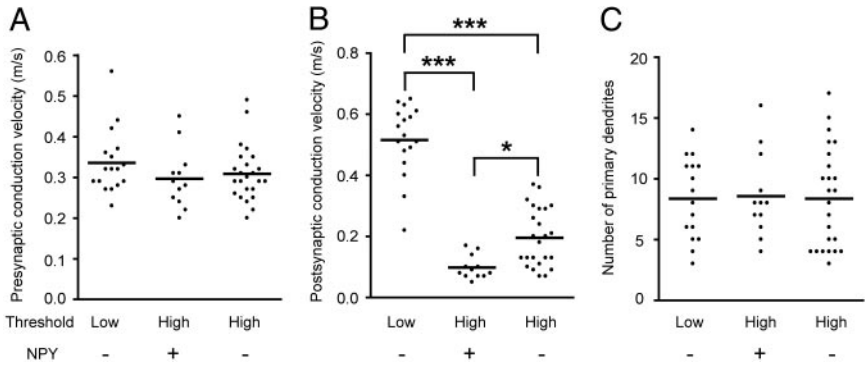

FIG. 7. Comparison of axonal conduction velocities and dendrite number in the three cell types. Scatter plots compare the distribution in each neuronal type of presynaptic conduction velocities (*A*), postsynaptic conduction velocities (*B*), and the number of primary dendrites (*C*). For each property, every cell is represented as a single point and horizontal bars denote the population mean. For the purpose of visual clarity, the data points for each group are also spread horizontally. The only statistically significant differences between cell types were in postsynaptic conduction velocities; ***, $P < 0.001$; *, $P < 0.05$. Means and SD for these data are in Table 2.

confocal images (Fig. 6). The rationale for this approach relied on previous studies of the SCG from several mammalian species, which demonstrate a systematic correlation between nicotinic convergence and the number of primary dendrites (Purves and Lichtman 1985). We observed that the number of dendrites ranged from 3 to 17 with an overall average of 8.4 ± 3.7 ($n = 53$), which agrees with the earlier assessment of the rat SCG (Purves and Lichtman 1985). There were, however, no differences among the three cell groups classified on the basis of stimulus threshold and NPY expression. The cells in each group had a similar range and average number of primary dendrites (Figs. 6 and 7*C*, Table 2).

Three cell types differ in size

In sympathetic ganglia of the bullfrog, mouse, and guinea pig, cell body size can correlate with phenotypic identity (Dodd and Horn 1983a; Gibbins 1991; Gibbins et al. 1996). The possibility that a similar relation exists in the rat SCG is suggested by the observation that NPY-negative neurons in the caudal ganglion are ~6 μm larger in diameter than NPY-positive neurons (Headley et al. 2005). When we compared ECN projecting neurons that had been classified using presynaptic stimulus threshold and NPY expression, it revealed significant size differences among all three cell types (Table 2). Low-threshold, NPY-negative neurons were the largest cells with a mean diameter of 33 μm, high-threshold, NPY-negative neurons were intermediate in size with a mean diameter of 29 μm, and high-threshold, NPY-positive neurons were the smallest cells with a mean diameter of 25 μm.

DISCUSSION

This paper shows for the first time that three types of sympathetic neuron can be identified in the rat SCG using the combined criteria of antidromic activation, presynaptic stimulus threshold, and NPY expression. The analysis has focused on neurons in the caudal portion of the ganglion that project to targets in the jaw and neighboring regions of the head by way of the external carotid nerve. In light of other knowledge describing the cellular organization of the SCG, it is proposed that low-threshold, NPY-negative cells are secretomotor neurons that supply salivary glands, that high-threshold, NPY-positive cells are vasoconstrictor neurons, and that high-threshold, NPY-negative cells are pilomotor neurons. Development of this scheme for neuronal identification in the isolated SCG opens the possibility of studying mechanisms of ganglionic integration that are specialized for different sympathetic modalities.

Origin of a new scheme for cellular identification

Our approach to neuronal identification in the rat SCG draws on previous studies of other ganglia. In the early 1960s, it was discovered that neurons in amphibian paravertebral ganglia can be classified as B and C cells by their axonal conduction velocities (Nishi et al. 1965). This provided a starting point for comparing cell types that led to many discoveries. B cells are larger than C cells (Dodd and Horn 1983a; Jan and Jan 1982; Nishi et al. 1965). B and C cells innervate different end organs (Jobling and Horn 1996; Thorne and Horn 1997), and they express different muscarinic synaptic mechanisms (Brown and Adams 1980; Dodd and Horn 1983b; Shen and Horn 1996; Smith 1994) and different neuropeptides (Horn and Stofer 1989; Horn et al. 1987; Jan and Jan 1982). Importantly, some of these features have parallels in the mammalian sympathetic system.

In the cat, lumbar paravertebral ganglia contain functional subsystems of sympathetic neurons that control different end organs (Janig and McLachlan 1992; Janig and Szulczyk 1981). These phenotypes are activated through different reflexes in the

TABLE 2. *Properties of neurons projecting to the ECN*

Cell Type	*n*	Presynaptic Conduction Velocity, m/s	Postsynaptic Conduction Velocity, m/s	Overall Conduction Velocity, m/s	Cell Body Diameter, μm	Number of Primary Dendrites
Low threshold/NPY−	17	0.34 ± 0.08	0.52 ± 0.12	0.36 ± 0.07	33.40 ± 3.47	8.4 ± 3.3
High threshold/NPY+	12	0.30 ± 0.07	0.10 ± 0.04	0.22 ± 0.05	25.40 ± 2.88	8.6 ± 3.3
High threshold/NPY−	24	0.31 ± 0.10	0.20 ± 0.10	0.27 ± 0.06	29.34 ± 6.03	8.4 ± 4.2

Pre- and postsynaptic conduction velocities were calculated from intracellular latency measurements at room temperature as illustrated in Fig. 5. Overall conduction velocities were calculated for each cell by combining the pre- and postsynaptic conduction distances and dividing it by the combined latency. The cell-type specific differences in postsynaptic conduction velocity, overall conduction velocity, and diameter were statistically significant. Differences in presynaptic conduction velocity and number of primary dendrites were not significant. Values are means ± SD.

intact animal, and they are characterized by distinct pre- and postganglionic axonal conduction velocities. Feline preganglionic axons are generally B fibers that conduct at 1–10 m/s, and most postganglionic axons are C fibers that conduct at <1 m/s. As in frogs and toads, vasoconstrictors in the cat have the slowest pre- and postganglionic conduction velocities.

We found that almost all postganglionic axons in the rat SCG were C fibers, even at physiological temperatures. Warming the ganglion from room temperature to 35°C caused a doubling of the slowest and fastest components of the compound action potential from 0.21 and 0.40 m/s to 0.42 and 0.87 m/s (Table 1). Using this result and the single-cell data, one can see that about half of the postganglionic fibers belonging to low-threshold neurons were borderline B fibers—doubling the intracellular estimates of their conduction velocities at room temperature indicates that at physiological temperature they would conduct at 1–1.4 m/s (Table 2, Fig. 7, *A* and *B*). This differed from preganglionic fibers, which all behaved as C fibers, and was in marked contrast to the B fibers commonly observed in preganglionic sympathetic axons of the cat (Janig and Szulczyk 1981).

In our experiments, stimulus threshold proved to be a more sensitive criterion than conduction velocity for distinguishing between subpopulations of preganglionic axons. One possible explanation for the inability to distinguish between the presynaptic conduction velocities of low- and high-threshold neurons is that high-threshold neurons can also have low-threshold inputs. Although these synapses are too weak to drive action potentials, they could in some cases have led to underestimates of the conduction latencies for high-threshold fibers.

In addition to making it more difficult to measure presynaptic latencies, the finding that some cells receive combined low- and high-threshold input raises an important physiological question. Does this observation indicate that different functional classes of preganglionic fibers converge on individual ganglion cells or might it simply reflect the technical limitations of isolating subtle differences between populations of preganglionic fibers whose stimulus thresholds overlap? At this time, we cannot rule out the possibility of preganglionic cross-talk between sympathetic modalities. If it exists, then this would represent a clear departure from the case of B and C cells in amphibian paravertebral ganglia, which receive separate preganglionic inputs (Dodd and Horn 1983a; Horn and Stofer 1988; Skok 1973; Smith 1994).

Relation to secretomotor, pilomotor, and vasoconstrictor neurons

Support for the proposed functional identification of low- and high-threshold neurons in the caudal SCG comes from previous work that combined retrograde axonal tracing with cell counts and immunocytochemistry. From retrograde tracing, it is clear that neurons in the caudal SCG project selectively into the ECN and that neurons in the rostral SCG project selectively into the ICN (Bowers and Zigmond 1979). For purposes of intracellular neuronal identification, the present study focused on neurons the ECN projection of which was confirmed by antidromic stimulation (Figs. 3 and 5). The largest groups of ECN projecting neurons consist of vasoconstrictors, piloerectors, and secretomotor neurons that control salivary glands. We propose that low-threshold neurons are secretomotor salivary neurons because they had the largest cell bodies and the fastest antidromic conduction velocities and were NPY negative (Figs. 4, 5, and 7, Table 2). Retrograde tracing from the salivary glands labels ~16% of rat SCG neurons (Voyvodic 1989). Cells labeled this way are among the largest, and 95% of them are NPY negative (Andrews et al. 1996; Grkovic and Anderson 1997). This contrasts with NPY-positive sympathetic neurons, which for the most part are vasoconstrictors (Jarvi et al. 1986; Lundberg et al. 1982, 1984). Three exceptions to this generalization are neurons that innervate the iris, pineal gland, and thyroid gland (Bjorklund et al. 1985; Bowers et al. 1984; Flett and Bell 1991; Grkovic et al. 1999; Grunditz et al. 1984; Reuss and Moore 1989; Sundler et al. 1989). However, each of these phenotypes constitutes only 1–2% of SCG neurons, and those supplying the iris and pineal leave the SCG through the ICN. For these reasons, it seems most likely that the high-threshold NPY-positive neurons projecting to the ECN were primarily vasoconstrictors. Other properties of these neurons also match the known features of vasoconstrictors. As in the mouse, cat, and bullfrog (Dodd and Horn 1983b; Gibbins 1991; Janig and Szulczyk 1981), NPY-positive rat neurons had the smallest cell bodies and the slowest postganglionic axonal conduction velocities (Table 2, Fig. 7*B*). Finally, it seems most likely that high-threshold NPY-negative cells are pilomotor in function based on their similarity to sympathetic neurons in the mouse and cat. Piloerectors in the mouse SCG are NPY-negative, intermediate in size, and relatively abundant, probably constituting 20% of all cells (Gibbins 1991). Feline piloerector neurons have faster postganglionic conduction velocities than vasoconstrictors (Janig and McLachlan 1992; Janig and Szulczyk 1981).

In our study, the number of neurons representing each of the three cell types did not reflect their relative abundance in the intact ganglion. Thus for example, 32% of the cells in Table 2 are putative secretomotor neurons, but this group only represents ~16% of SCG neurons (Voyvodic 1989) and 23% of the cells are putative vasoconstrictors, but this group represents about half of SCG neurons (Jarvi et al. 1986). These disparities arise largely from the fact that it is more difficult to record from small cells than large cells. Low-threshold NPY-negative neurons proved to be the largest cells, probably accounting for why they are overrepresented in our sample. High-threshold NPY-positive neurons were the smallest cells, which contributed to their underrepresentation. In addition, we cannot rule out the possibility that the process of filling cells damaged them and caused some false negative results in the immunocytochemistry. However, we do not think this can explain the fact that 17 of 17 low-threshold cells were NPY negative. Similarly, impalement damage may have confounded the high-threshold data to some degree but not enough to obscure significant differences between NPY-positive and -negative neurons in terms of their sizes and axonal conduction velocities (Table 2).

Implications for ganglionic integration

A key goal of the present experiments was to compare nicotinic convergence in different sympathetic phenotypes. Although previous work has examined systematically the variations in convergence that occur in different mammalian species (Purves and Hume 1981; Purves and Lichtman 1985), the

physiological role of this diversity remains enigmatic. In a recently developed theory of ganglionic integration, it has been proposed that nicotinic convergence enables sympathetic ganglia to function as synaptic amplifiers of preganglionic activity (Karila and Horn 2000; Wheeler et al. 2004). If one was to observe cell-specific differences in convergence, then it would suggest that gain varies in different sympathetic modalities. When this hypothesis was tested by comparing the number of primary dendrites in putative secretomotor, vasoconstrictor, and pilomotor neurons (Figs. 6 and 7*C,* Table 2), the results showed clearly that all three cell types were similar. This finding supports the results from two other studies using somewhat different approaches. In the first, guinea pig lumbar sympathetic vasoconstrictor and pilomotor neurons were filled with neurobiotin and classified on the basis of NPY expression (Gibbins and Matthew 1996). In the second, rat SCG neurons projecting to the middle cerebral artery, submandibular gland, and iris were back labeled and then injected in fixed tissue (Andrews et al. 1996). Although all of these studies indicate that the number of primary dendrites is unrelated to the phenotypic identity, it is important to note that other mechanisms could generate phenotypic specialization of nicotinic integration. This diversity could arise, for example, through selective developmental regulation of synaptic strength and also through mechanisms of short-term plasticity such as facilitation, depression and metabotropic modulation (Karila and Horn 2000; Wheeler et al. 2004). Pursuit of these possibilities is now feasible using the scheme for neuronal identification presented in this paper.

ACKNOWLEDGMENTS

We thank Drs. Ian Gibbins and Paul Kullmann for many helpful discussions.

GRANTS

This work was supported by National Institute of Neurological Disorders and Stroke Grant NS-21065 and by a predoctoral fellowship to C. Li from the Pennsylvania Delaware Affiliate of the American Heart Association.

REFERENCES

Andrews TJ, Thrasivoulou C, Nesbit W, and Cowen T. Target-specific differences in the dendritic morphology and neuropeptide content of neurons in the rat SCG during development and aging. *J Comp Neurol* 368: 33–44, 1996.

Arbab MA, Wiklund L, and Svendgaard NA. Origin and distribution of cerebral vascular innervation from superior cervical, trigeminal and spinal ganglia investigated with retrograde and anterograde WGA-HRP tracing in the rat. *Neuroscience* 19: 695–708, 1986.

Bjorklund H, Hokfelt T, Goldstein M, Terenius L, and Olson L. Appearance of the noradrenergic markers tyrosine hydroxylase and neuropeptide Y in cholinergic nerves of the iris following sympathectomy. *J Neurosci* 5: 1633–1640, 1985.

Bowers CW, Dahm LM, and Zigmond RE. The number and distribution of sympathetic neurons that innervate the rat pineal gland. *Neuroscience* 13: 87–96, 1984.

Bowers CW and Zigmond RE. Localization of neurons in the rat superior cervical ganglion that project into different postganglionic trunks. *J Comp Neurol* 185: 381–391, 1979.

Brown DA and Adams PR. Muscarinic suppression of a novel voltage-sensitive K^+ current in a vertebrate neuron. *Nature* 283: 673–676, 1980.

Dodd J and Horn JP. A reclassification of B and C neurons in the ninth and tenth paravertebral sympathetic ganglia of the bullfrog. *J Physiol* 334: 255–269, 1983a.

Dodd J and Horn JP. Muscarinic inhibition of sympathetic C neurons in the bullfrog. *J Physiol* 334: 271–291, 1983b.

Eccles JC. The action potential of the superior cervical ganglion. *J Physiol* 85: 179–206, 1935.

Feldberg W and Gaddum JH. The chemical transmitter at synapses in a sympathetic ganglion. *J Physiol* 81: 305–319, 1934.

Flett DL and Bell C. Topography of functional subpopulations of neurons in the superior cervical ganglion of the rat. *J Anat* 177: 55–66, 1991.

Gibbins IL. Vasomotor, pilomotor and secretomotor neurons distinguished by size and neuropeptide content in superior cervical ganglia of mice. *J Auton Nerv Syst* 34: 171–183, 1991.

Gibbins I. Peripheral autonomic pathways. In: *The Human Nervous System* (2nd ed.), edited by Paxinos G and Mai J. Oxford: Elsevier Academic, 2004, p. 134–189.

Gibbins IL and Matthew SE. Dendritic morphology of presumptive vasoconstrictor and pilomotor neurons and their relations with neuropeptide-containing preganglionic fibers in lumbar sympathetic ganglia of guinea pigs. *Neuroscience* 70: 999–1012, 1996.

Gibbins IL, Matthew SE, Bridgman N, and Morris JL. Sympathetic vasoconstrictor neurons projecting from the guinea-pig superior cervical ganglion to cutaneous or skeletal muscle vascular beds can be distinguished by soma size. *Neurosci Lett* 213: 197–200, 1996.

Grkovic I and Anderson CR. Calbindin D28K-immunoreactivity identifies distinct subpopulations of sympathetic pre- and postganglionic neurons in the rat. *J Comp Neurol* 386: 245–259, 1997.

Grkovic I, Edwards SL, Murphy SM, and Anderson CR. Chemically distinct preganglionic inputs to iris-projecting postganglionic neurons in the rat: a light and electron microscopic study. *J Comp Neurol* 412: 606–616, 1999.

Grunditz T, Hakanson R, Rerup C, Sundler F, and Uddman R. Neuropeptide Y in the thyroid gland: neuronal localization and enhancement of stimulated thyroid hormone secretion. *Endocrinology* 115: 1537–1542, 1984.

Headley DB, Suhan NM, and Horn JP. Rostro-caudal variations in neuronal size reflect the topography of cellular phenotypes in the rat superior cervical sympathetic ganglion. *Brain Res* 1057: 98–104, 2005.

Hirst GD and McLachlan EM. Development of dendritic calcium currents in ganglion cells of the rat lower lumbar sympathetic chain. *J Physiol* 377: 349–368, 1986.

Horn JP and Stofer WD. Spinal origins of preganglionic B and C neurons that innervate paravertebral sympathetic ganglia nine and ten of the bullfrog. *J Comp Neurol* 268: 71–83, 1988.

Horn JP and Stofer WD. Preganglionic and sensory origins of calcitonin gene-related peptide-like and substance P-like immunoreactivities in bullfrog sympathetic ganglia. *J Neurosci* 9: 2543–2561, 1989.

Horn JP, Stofer WD, and Fatherazi S. Neuropeptide Y-like immunoreactivity in bullfrog sympathetic ganglia is restricted to C cells. *J Neurosci* 7: 1717–1727, 1987.

Jan LY and Jan YN. Peptidergic transmission in sympathetic ganglia of the frog. *J Physiol* 327: 219–246, 1982.

Janig W and McLachlan EM. Characteristics of function-specific pathways in the sympathetic nervous system. *Trends Neurosci* 15: 475–481, 1992.

Janig W and Szulczyk P. The organization of lumbar preganglionic neurons. *J Auton Nerv Syst* 3: 177–191, 1981.

Jarvi R, Helen P, Pelto-Huikko M, and Hervonen A. Neuropeptide Y (NPY)-like immunoreactivity in rat sympathetic neurons and small granule-containing cells. *Neurosci Lett* 67: 223–227, 1986.

Jobling P and Gibbins IL. Electrophysiological and morphological diversity of mouse sympathetic neurons. *J Neurophysiol* 82: 2747–2764, 1999.

Jobling P and Horn JP. In vitro relation between preganglionic sympathetic stimulation and activity of cutaneous glands in the bullfrog. *J Physiol* 494: 287–296, 1996.

Karila P and Horn JP. Secondary nicotinic synapses on sympathetic B neurons and their putative role in ganglionic amplification of activity. *J Neurosci* 20: 908–918, 2000.

Keynes RD and Aidley DJ. *Nerve and Muscle.* Cambridge: Cambridge, 1991.

Langley JN. On the origin from the spinal cord of the cervical and upper thoracic sympathetic fibers, with some observations on white and grey rami communicantes. *Philos Trans R Soc Lond B Biol Sci* 183: 85–124, 1892.

Lundberg JM, Saria A, Anggard A, Hokfelt T, and Terenius L. Neuropeptide Y and noradrenaline interaction in peripheral cardiovascular control. *Clin Exp Hypertens A* 6: 1961–1972, 1984.

Lundberg JM, Terenius L, Hokfelt T, Martling CR, Tatemoto K, Mutt V, Polak J, Bloom S, and Goldstein M. Neuropeptide Y (NPY)-like immunoreactivity in peripheral noradrenergic neurons and effects of NPY on sympathetic function. *Acta Physiol Scand* 116: 477–480, 1982.

McLachlan EM, Davies PJ, Habler HJ, and Jamieson J. On-going and reflex synaptic events in rat superior cervical ganglion cells. *J Physiol* 501: 165–181, 1997.

McLachlan EM, Habler HJ, Jamieson J, and Davies PJ. Analysis of the periodicity of synaptic events in neurons in the superior cervical ganglion of anesthetized rats. *J Physiol* 511: 461–478, 1998.

Morris JL, Zhu BS, Gibbins IL, and Blessing WW. Subpopulations of sympathetic neurons project to specific vascular targets in the pinna of the rabbit ear. *J Comp Neurol* 412: 147–160, 1999.

Nishi S, Soeda H, and Koketsu K. Studies on sympathetic B and C neurons and patterns of pregnaglionic innervation. *J Cell Physiol* 66: 19–32, 1965.

Purves D and Hume RI. The relation of postsynaptic geometry to the number of presynaptic axons that innervate autonomic ganglion cells. *J Neurosci* 1: 441–452, 1981.

Purves D and Lichtman JW. Geometrical differences among homologous neurons in mammals. *Science* 228: 298–302, 1985.

Rat Genome Sequencing Project Consortium. Genome sequence of the Brown Norway rat yields insights into mammalian evolution. *Nature* 428: 493–521, 2004.

Reuss S and Moore RY. Neuropeptide Y-containing neurons in the rat superior cervical ganglion: projections to the pineal gland. *J Pineal Res* 6: 307–316, 1989.

Shen WX and Horn JP. Presynaptic muscarinic inhibition in bullfrog sympathetic ganglia. *J Physiol* 491: 413–421, 1996.

Skok VI. *Physiology of Autonomic Ganglia.* Tokyo: Igaku Shoin, 1973.

Skok VI and Ivanov AY. What is the ongoing activity of sympathetic neurons? *J Auton Nerv Syst* 7: 263–270, 1983.

Smith PA. Amphibian sympathetic ganglia: an owner's and operator's manual. *Prog Neurobiol* 43: 439–510, 1994.

Sundler F, Grunditz T, Hakanson R, and Uddman R. Innervation of the thyroid. A study of the rat using retrograde tracing and immunocytochemistry. *Acta Histochem Suppl* 37: 191–198, 1989.

Thorne R and Horn JP. Role of ganglionic cotransmission in sympathetic control of the isolated bullfrog aorta. *J Physiol* 498: 201–214, 1997.

Uddman R, Hara H, and Edvinsson L. Neuronal pathways to the rat middle meningeal artery revealed by retrograde tracing and immunocytochemistry. *J Auton Nerv Syst* 26: 69–75, 1989.

Voyvodic JT. Peripheral target regulation of dendritic geometry in the rat superior cervical ganglion. *J Neurosci* 9: 1997–2010, 1989.

Wheeler DW, Kullmann PH, and Horn JP. Estimating use-dependent synaptic gain in autonomic ganglia by computational simulation and dynamic-clamp analysis. *J Neurophysiol* 92: 2659–2671, 2004.